How nutrients shape antibiotic sensitivity of Pseudomonas aeruginosa: food for thought

Kok, M.

Section II

Nutrients shape antibiotic sensitivity

How nutrients shape antibiotic sensitivity in *Pseudomonas aeruginosa*

Food for thought

Chapter 3

Nutrient conditions affect antimicrobial pharmacodynamics in *Pseudomonas aeruginosa*

Maik Kok, Thomas Hankemeier, Coen van Hasselt

Microbiology Spectrum, 2025, 13(1), e01409-24

Abstract

The infectious microenvironment in chronic respiratory tract infections is characterized by substantial variability in nutrient conditions, which may impact colonization and treatment response of pathogens. Metabolic adaptation of the CF-associated pathogen *Pseudomonas aeruginosa* has been shown to lead to changes in antibiotic sensitivity. The impact of specific nutrients on the response to antibiotics is, however, poorly characterized. Here, we investigated how different carbon sources impact the antimicrobial pharmacodynamic responses in *P. aeruginosa*. We evaluated the effect of six antibiotics (aztreonam, ceftazidime, ciprofloxacin, colistin, imipenem, tobramycin) on *P. aeruginosa* cultured in a basal medium enriched for seven different carbon sources (alanine, arginine, aspartate, glucose, glutamate, lactate, proline). Pharmacodynamic responses were characterized by measuring time-kill profiles for a bioluminescent *P. aeruginosa* PAO1 *Xen41* strain. We show that single-nutrient modifications minimally affected bacterial growth rate. For specific nutrient-antibiotic combinations, we find relevant alterations in antibiotic sensitivity (i.e., EC_{50}) and the maximum drug effect (E_{max}), in particular for ciprofloxacin, colistin, imipenem and tobramycin. The most pronounced effect was observed for tobramycin, where glucose was found to reduce the EC_{50} (0.5-fold) while lactate-enriched conditions led to a 4.3-fold increase in EC_{50}. Using pharmacokinetic-pharmacodynamic simulations, we illustrate that the magnitude of the nutrient-driven pharmacodynamic changes impact treatment for clinical dosing strategies of tobramycin. In summary, this study underscores the impact of nutrient composition on antimicrobial pharmacodynamics, which could potentially contribute to observed variability of antimicrobial treatment responses in CF patients.

Importance

Chronic respiratory tract infections in cystic fibrosis patients present significant challenges for antibiotic treatment due to the complexity of the respiratory environment. This study investigated how variations in nutrient levels, altered during chronic infections, affect pathogen response to antibiotics in an experimental setting. By simulating different nutrient conditions, we aimed to uncover interactions between nutrient availability and antibiotic sensitivity. Our findings provide critical insights that could lead to more effective treatment strategies for managing chronic respiratory tract infections in cystic fibrosis patients, while also guiding future research in improving treatment methodologies.

3.1. Introduction

Cystic fibrosis (CF) associated lung infections are facilitated by a complex infectious microenvironment involving a dense mucus layer harboring a diverse array of potential microbial nutrients[1]. Antibiotic treatment in patients with CF often yields unpredictable outcomes and aligns poorly with routine antimicrobial susceptibility testing[2,3]. Profound variability in microbial nutrients is observed within the chronic infectious environment, both across and within patients[4,5]. Unlike many other bacterial pathogens, *Pseudomonas aeruginosa* prioritizes the utilization of a wide array of carbon sources over glucose, including alanine, arginine, aspartate, glutamate, proline, and lactate[6,7]. This metabolic versatility may explain its pervasive presence in chronic CF-associated infections, and provides a competitive advantage during antibiotic treatment[8–10].

Alterations in metabolic processes associated with differences in available nutrients may impact response to antibiotic treatment in *P. aeruginosa*[11–13]. For example, nutrient deprivation prevents cell wall modifications due to its high energy demand, enhancing the effect of cell wall targeting antibiotics (e.g., polymyxins and β-lactams)[14–16]. The supplementation of metabolites to activate energy production through aerobic respiration in nutrient-deprived environments can increase sensitivity towards fluoroquinolones and aminoglycosides[17–19]. While these changes illustrate the modulatory role of deprived nutrient conditions and microbial metabolism on the response to antibiotics, insights into the contribution of nutrients relevant to CF lung microenvironments remain limited.

To assess the effects of nutrient conditions on antimicrobial pharmacodynamics (PD), conventional readouts such as minimum inhibitory concentrations (MIC) have important limitations, as this is a static composite measure. More comprehensive characterization of changes in the pharmacodynamic response to antibiotics can be achieved through time kill studies, which monitor bacterial densities over time when exposed to antibiotics, allowing the evaluation of bacterial growth, antibiotic-associated killing, and adaptation effects[20,21]. Although time-kill studies provide these valuable insights, they remain limited in their throughput and the number of time points at which data can be collected[22]. The use of bacterial strains carrying luminescent reporters allows real-time monitoring of bacterial growth and killing dynamics during antibiotic exposure[23,24]. The resulting profiles can be analyzed using mathematical pharmacodynamic models to obtain further quantitative insights into PD relationships. As such, the use of luminescence-based time kill studies in combination with quantitative pharmacodynamic models is well-suited for comprehensively assessing the effects of nutrient conditions on antibiotic response.

In the current study, we aimed to systematically evaluate the impact of a wide range of CF sputum-relevant carbon sources on antimicrobial time-kill responses in *P. aeruginosa*. The nutrients evaluated included alanine, arginine, aspartate, glutamate, lactate, proline, and glucose. These nutrient-associated effects were evaluated for six antibiotics commonly used for respiratory tract infections in CF, including aztreonam, ceftazidime, ciprofloxacin, colistin, imipenem, and tobramycin. We assessed the bacterial growth/kill time course profiles using extensive time-kill studies with a modified *P. aeruginosa* PAO1 strain carrying a constitutively active luminescent reporter. This strain was subsequently used to infer PD parameters and perform pharmacokinetic-pharmacodynamic (PK-PD) simulations to demonstrate the potential clinical impact of nutrients on antimicrobial PD.

3.2. Materials and Methods

Culture media and bacterial strain

A basal medium was prepared consisting of physiologically relevant concentrations of amino acids in synthetic CF sputum as described previously[7], calcium and magnesium adjusted 0.11 M phosphate buffer, ammonium chloride, potassium nitrate, ferrous sulfate, Basal Medium Eagle 1x vitamins, and trace metals. The pH of the basal medium was confirmed to be 7.4, and was verified after addition of nutrients and filter sterilization. The specific concentrations of all medium components are listed in **Table S1**. We then prepared 7 unique nutrient-specific media for each of the carbon sources used in this study, including alanine, arginine, aspartate, glutamate, glucose, proline, and lactate. Each of these nutrients was added separately to the basal medium in excess at a concentration of 15 mM. The *P. aeruginosa* bioluminescent strain PAO1 Xen41 (Revvity Inc., Waltham, MA, USA) was used in all experiments. The promoterless insertion of the *luxCDABE* cassette into the chromosomal genome resulted in a linear relationship between luminescence in relative light units (RLU) and CFU/mL (**Figure S1**)[23,24].

Antibiotics

Antibiotic stock solutions were freshly prepared on the day of the experiment and diluted to desired concentrations using an Opentrons OT-2 (Opentrons Inc., New York, NY, USA) liquid handling system. Aztreonam and ceftazidime pentahydrate were purchased from Thermo Fisher Scientific (Breda, The Netherlands). Ciprofloxacin, imipenem monohydrate, and tobramycin were purchased from Chem-Impex International (Wood Dale, IL, USA). Colistin sulfate was purchased from Cayman Chemical Company (Ann Arbor, MI, USA).

Experimental workflow

Time-kill assays were conducted by culturing *P. aeruginosa* in each of the nutrient-specific media formulations and exposing the cultures to 6 different antibiotics. We tested 9 different serially diluted concentrations in a microtiter plate format, centered around their minimal inhibitory concentrations (**Figure 1**). All experiments were conducted at 37 °C and with shaking at 150 rpm.

The PAO1 Xen41 strain was streaked on LB agar plates and incubated overnight. One colony was transferred to a nutrient specific media formulation (4 mL) and cultured overnight. The liquid cultures were diluted to an optical density at 600 nm (OD_{600}) of 0.05 before inoculation, corresponding to an approximate bacterial concentration of $5*10^6$ CFU/mL. The bacterial inoculum (50 µL) was added to fresh medium with antibiotics (150 µL) in a white 96-well microtiter plate.

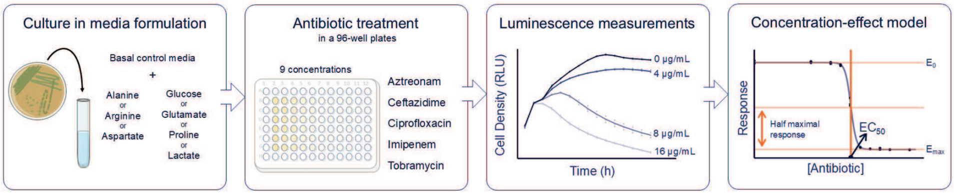

Figure 1. Experimental approach. The experiment started with by a liquid culture in the media formulation containing 1 or none of the nutrients of interest. The population was diluted to the starting density and treated with 9 concentrations of antibiotic while the luminescence was determined every hour in relative light units (RLU). A four parameter log-logistic function was fitted on the area under the curve or growth rate per antibiotic concentration to determine the upper limit (E_0), lower limit (E_{max}), and half-maximal effective concentration (EC_{50}).

After inoculation, microtiter plates were transferred to a Liconic StoreX STX44 incubator (Mauren, Principality of Liechtenstein) for incubation (95% relative humidity). A Peak Analysis and Automation KX-2 Laboratory Robot (Hampshire, United Kingdom) transferred the microtiter plate every hour between the incubator and the BMG Labtech Fluostar Omega microplate reader (Ortenberg, Germany) for time-course data acquisition. The density of viable bacteria was determined by measuring luminescence, quantified as relative light units (RLU).

Data processing and analysis

All data preprocessing and analyses are performed using R. To evaluate fitness differences between growth media, the maximal population growth rates (μ_{max}) and the maximal population density (N_{max}) under antibiotic free culture conditions were calculated using the all splines function from the grofit package[25]. Differences in growth parameters in the studied media formulations compared to the basal media were assessed by the Dunnett's Test from the DescTools R package[26].

To quantify drug effects, the total bacterial burden was determined by calculating the area under the curve (AUC) of the RLU between 1 and 15 hours of incubation (**Figure S2**). The resulting AUC values were then used to quantify pharmacodynamic parameters. We fitted for each antibiotic-nutrient combination the mean (n=3) AUC to the antibiotic concentration ([AB]) using a four parameter log-logistic (LL.4) function from the drc R package (**Equation 1**)[27]. This function includes parameters for the hill coefficient (n_H), the lower limit (E_{max}), the upper limit (E_0), and the relative half-maximal effective concentration (EC_{50}). The difference in relative EC_{50} among culture conditions was quantified using the 95% confidence interval.

$$AUC([AB]) = E_{max} + \frac{E_0 - E_{max}}{1 + e^{n_H(\log([AB]) - \log(EC_{50}))}} \qquad (1)$$

Pharmacokinetic-pharmacodynamic (PK-PD) simulations

We used a previously published pharmacokinetic (PK) model for tobramycin to perform PK-PD simulations[28]. We simulated the clinical concentration-time profiles for a typical dose of 3.3 mg/kg of intravenous tobramycin, administered every 8 hours (**Table S2**). Interpatient variability for the parameters was derived from published interquartile ranges. Antibiotic PD was described by first estimating growth/kill rates for each antibiotic concentration, which were subsequently fitted to a pharmacodynamic sigmoidal function relation antibiotic growth/kill rate to antibiotic concentration. The growth rates where determined by determining the slope of the phase of the luminescence time kill curve where the drug effect occurred (**Figure S6**), using the grofit package.

3.3. Results

Nutrient-dependent shift in antibiotic sensitivity.

We cultured *P. aeruginosa* under various nutrient conditions in the presence of different antibiotics to investigate the effect of nutrients on the pharmacodynamic (PD) response. To summarize the bacterial response kinetics–encompassing growth enhancement, suppression, or killing during antibiotic treatment–we calculated the AUC of the luminescence time course profiles. We then regressed the AUC values against antibiotic concentrations using a sigmoidal Emax model, allowing us to visualize differences in the pharmacodynamic response across conditions (**Figure 2**). Overall, these analyses revealed significant effects of nutrients on the antibiotic concentration required to achieve

50% of the total antimicrobial effect (relative EC_{50}), and the steepness of the concentration-response profiles (**Figure S3**).

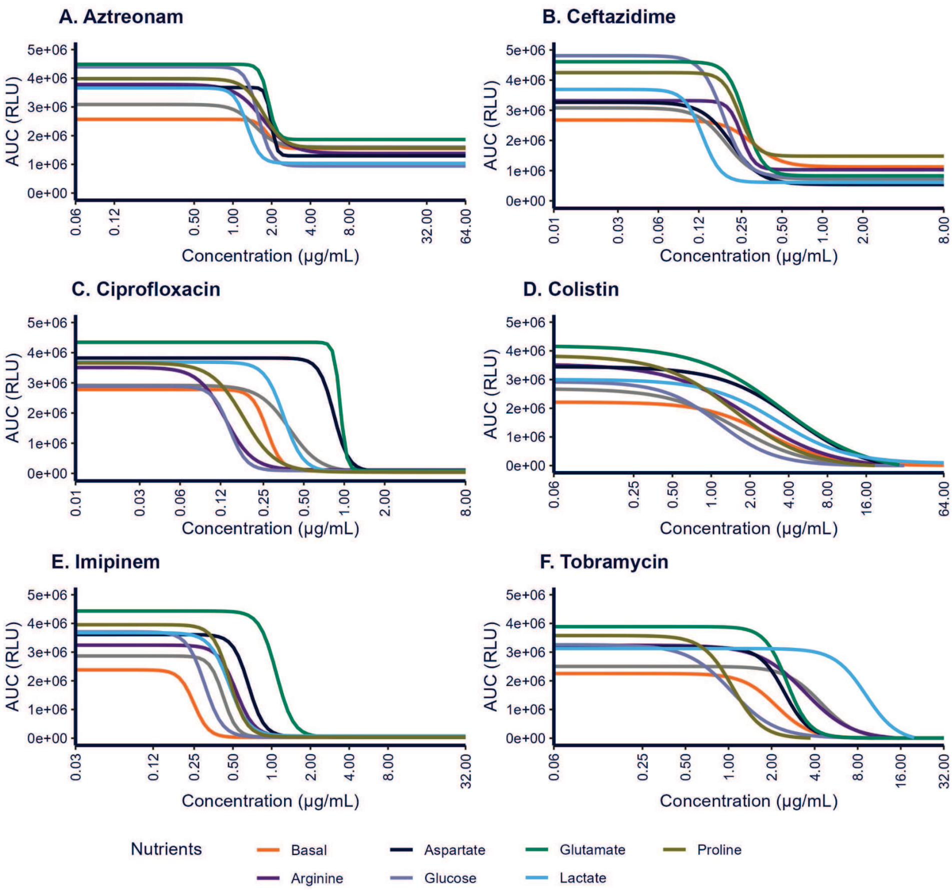

Figure 2. Pharmacodynamic exposure-response relationships for antibiotics cultured under different nutrient conditions. The area under the curve (AUC) for bacterial growth/kill based on relative light units (RLU) up to 15h in relation to antibiotic concentrations (n=9) were fitted using sigmoidal E_{max} curves, for different nutrient-enriched media formulations and the basal control media condition. The lines represent the mean predictions derived from 3 biological replicates (n = 3). Abbreviations: Aztreonam (AZT), ceftazidime (CAZ), ciprofloxacin (CIP), colistin (COL), imipenem (IMI), and tobramycin (TOB).

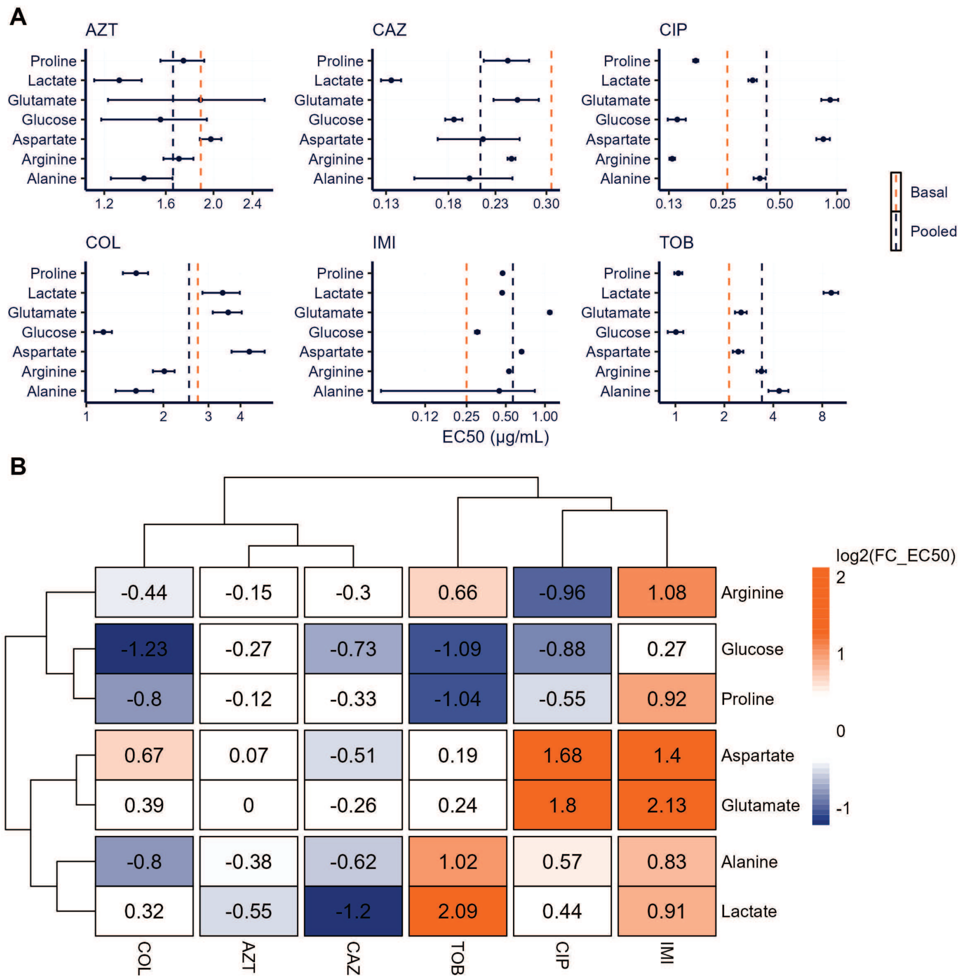

Figure 3. Changes in antibiotic sensitivity (EC_{50}) of P. aeruginosa across different nutrients and antibiotics. Observed area-under-the-curve for bacterial growth and kill for P. aeruginosa PAO1-Xen41 were regressed against drug concentrations for different antibiotics and nutrients, using a sigmoidal Emax function. The resulting EC_{50} estimates for different antibiotic-nutrient combinations are shown for (**A**) absolute EC50 values (mean and 95% confidence intervals), with vertical dashed lines indicating the EC50 obtained from the base media control treatment, and the cross-nutrient median EC_{50}, and (**B**) median fold-change (FC) values in EC_{50}, compared to the base media EC_{50}. The antibiotics and nutrients were clustered using Euclidean distance clustering to showcase patterns of antibiotic sensitivity and nutrient effect. Abbreviations: aztreonam (AZT), ceftazidime (CAZ), ciprofloxacin (CIP), colistin (COL), imipenem (IMI), and tobramycin (TOB).

The relative EC_{50} would be the primary metric of relevance to quantitatively indicate subtle changes in drug potency, i.e., antibiotic sensitivity across conditions. For several nutrient conditions, we observed clinically relevant alterations in the EC_{50} values across different antibiotics (**Figure 3A**). We observed both reductions in EC_{50} as compared to the basal media and increased EC_{50} values, indicating increased resistance. Across all antibiotics, no clear trends in EC_{50} shifts were observed for specific nutrients.

When comparing the relative change in EC_{50} to the basal medium (**Figure 3B**), both aztreonam and ceftazidime exhibited similarly enhanced sensitivity across different nutrient conditions. The most notable changes were the increased sensitivity observed in lactate-enriched media for both antibiotics. In contrast, imipenem sensitivity was consistently reduced in all nutrient-enriched conditions, with the most significant reductions observed in aspartate- and glutamate-enriched media. For ciprofloxacin, colistin and tobramycin a wider variation in effect was compared to the basal medium. Glucose- and proline-enriched media resulted in a reduction of EC_{50}, while aspartate, glutamate- and lactate-enriched media increased the EC_{50} for all three antibiotics. The largest change in sensitivity was observed for tobramycin, where for lactate-rich media, the EC_{50} value increased profoundly (log2(FC_EC50) = 2.09, a 4.4-fold increase).

Fitness differences in different culture conditions affect PD parameters.

We studied the effect of different nutrient-enriched media under antibiotic-free conditions on fitness and growth yield using the growth curve profiles (**Figure 4**), to understand their potential contributions to differences in antibiotic response. Except for alanine, for all nutrients we found an increase of >1.5 fold in the upper limit of the model (E_0), i.e., the antibiotic baseline with no antimicrobial effect used in our pharmacodynamic analyses (**Figure S3**). To further understand these effects we calculated the maximum population growth rate (μ_{max}) and the maximum population density (N_{max}) of antibiotic-free conditions (**Figure S4**). While the nutrient composition significantly affected μmax, the magnitude of the effect was modest (**Figure 4B**), with an increase of up to 1.2-fold compared to the basal control media observed only for aspartate and glutamate. The observed effects on E_0 are predominantly explained by differences in N_{max} (**Figure 4C**), with a >2-fold increase observed for aspartate and glutamate and a fold change

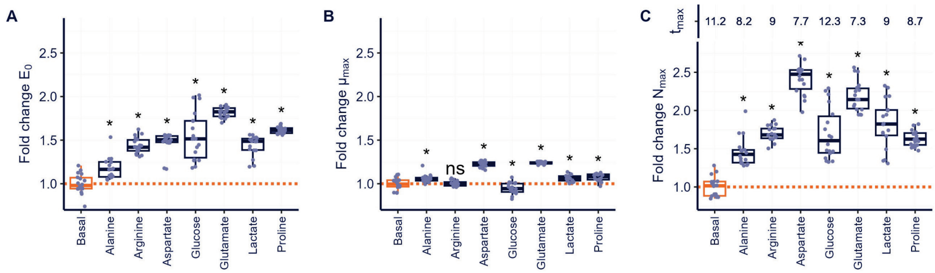

Figure 4. Nutrient effects on fitness and growth yield under antibiotic-free conditions. Growth curves for *P. aeruginosa* were analyzed for different media enriched for alanine, arginine, aspartate, glucose, glutamate, lactate, and proline on the fold change compared to basal media. (**A**) total growth yield described using the upper limit of the antibiotic concentration-response curve (E_0), (**B**) the maximal growth rate (μ_{max}) of the growth curve, (**C**) maximal population density (N_{max}) and the time (t_{max}) required to reach N_{max}. Significant changes compared to the basal control media are indicated using '*' for $p < 0.05$ and 'ns' for $p > 0.05$.

between 1.2 and 2.0 for all other nutrient conditions. Distinct differences in growth curves during the transition from the exponential growth phase to the stationary phase was visible (Figure S4), in particular for the time required to reach N_{max} (t_{max}).

The impact of differences in E_0 across different nutrient conditions on PD parameters was further evaluated by analyzing the total antimicrobial response. Comparing the relative EC_{50} with the absolute EC_{50} provides an indication of how the limits of PD model influence the total antimicrobial effect. The relative EC_{50} is defined as the midpoint between the two limits of concentration-response curve, whereas the absolute EC_{50} denotes a 50% reduction in the AUC from the baseline with no antimicrobial effect (E_0). A larger discrepancy between these EC_{50} values suggests a stronger impact of the two limits on determining the antibiotic EC_{50} [29]. For treatments with ciprofloxacin, colistin, imipenem and tobramycin, the difference between the average relative and absolute EC_{50} values was less than 5% (**Figure S5**). In contrast, ceftazidime and aztreonam treatments showed difference of respectively 14% and 22% indicating that differences in the PD model limits between the nutrient conditions do influence the determination of EC_{50}.

In vitro nutrient-driven PD differences impact treatment simulations with a clinically relevant tobramycin PK profile

To assess whether the magnitude of nutrient-associated changes in the PD response observed *in vitro* may have significance at clinically relevant antibiotic concentrations, we performed pharmacokinetic-pharmacodynamic (PK-PD) simulations. For proof of concept, we focused on tobramycin and the nutrients glucose and lactate, since for this antibiotic and these nutrient conditions clearly divergent PD effects were observed.

We re-fitted the PD model (**Equation 1**) with the in vitro obtained growth and kill rates from our luminescence time course data per antibiotic concentration. In the basal media enriched with glucose and lactate, maximum bacterial growth rates were similar (0.25 h^{-1} and 0.24 h^{-1}, respectively), as were the maximum bacterial kill rates (-0.15 h^{-1} and -0.14 h^{-1}, respectively) (**Figure S6**). However, the PD model estimated a 6-fold difference in the EC_{50} for glucose-enriched (1.4 µg/mL) and lactate-enriched (8.6 µg/mL) environments, indicating that tobramycin is profoundly more effective at lower concentrations in glucose-rich culture conditions.

We simulated clinical tobramycin concentration-time profiles using a previously published PK model for an intravenous dose of 3.3 mg/kg administered every 8 hours (**Figure 5A**). The tobramycin PK simulation shows that the free drug concentrations fell below the EC_{50} within 1 hour for glucose-rich conditions and within 5.5 hours for lactate-rich conditions after dose administration. As a result, treatment failure was observed for tobramycin under lactate-rich conditions, whereas growth suppression occurred in simulated glucose-enriched conditions (**Figure 5B**).

3.4. Discussion

In this study we used a combination of *in vitro* time-kill studies and mathematical modeling to investigate how specific nutrient conditions can distinctly affect bacterial growth and pharmacodynamic response of *P. aeruginosa* to different antibiotics.

We found that colistin, ciprofloxacin, imipenem and tobramycin demonstrated >2-fold differences in nutrient-dependent changes in antibiotic

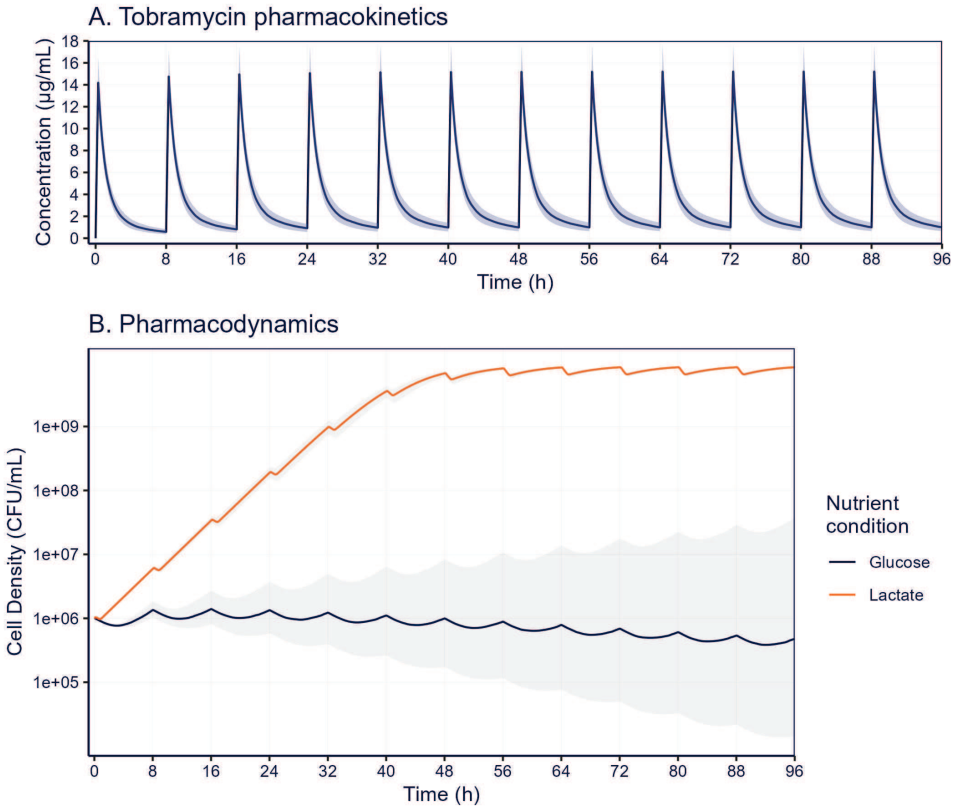

Figure 5. Pharmacokinetic and pharmacodynamic simulation of tobramycin treatment in glucose or lactate-rich environments. (**A**) Tobramycin concentrations are modelled using a two-compartment model following a 3.3 mg/kg q8h dosing regimen. (**B**) Treatment response is simulated using a pharmacodynamic model based on population growth rates per drug concentration from in vitro growth/kill curves. The solid lines represent the median (1000 simulations) with the interquartile range represented by the transparent-hued areas.

sensitivity (EC_{50}), while these nutrients only had a limited effect on changes in bacterial fitness. Our time-course analysis revealed that changes in growth dynamics induced by these antibiotics occur within the initial hours of treatment, even when nutrients are abundant and growth rates appear unchanged. This observation challenges the suggestion that antibiotic sensitivity changes were caused by nutrient depletion or diminished growth rates[30]. In contrast, the response to aztreonam and ceftazidime under various nutrient conditions was more complex, as both the baseline response (E_0) and the maximum antimicrobial effect (E_{max}) were differently affected by the various nutrients.

Our findings indicate that the adding glucose to nutrient-limited media enhances colistin sensitivity. Variations in colistin sensitivity under different nutrient conditions are thought to arise from nutrient-induced changes in cell wall structure[14,15]. Glucose-rich conditions have been previously suggested to decrease colistin sensitivity by stabilizing intracellular osmotic pressure[14]. Our finding of enhanced colistin sensitivity thus challenges the hypothesis of osmotic stabilization of glucose in nutrient-scarce conditions. This observation is consistent with documented increases in colistin sensitivity in minimal media supplemented with glucose[31].

We found a diminished sensitivity of imipenem under nutrient conditions involving arginine, aspartate, glutamate, or proline. This can be explained by reduced imipenem uptake due to porin competition with these amino acids. Indeed, imipenem susceptibility in *P. aeruginosa* relies on the presence of outer membrane porins, particularly OprD and OprP, which facilitate the diffusion of sugars and amino acids[32–34]. Furthermore, nutrient starvation upregulates OprD[32,33,35], providing an explanation for the increased imipenem sensitivity observed in both basal and glucose-rich media. The reduced growth rate and short exponential growth phase in these conditions may prompt an earlier starvation response, thereby enhancing OprD-mediated imipenem uptake.

We observed reduced ciprofloxacin susceptibility in glutamate media, which has previously been associated with adaptations in nitrogen metabolism and stress responses[36,37]. This metabolic adaptation mitigates ciprofloxacin's antibacterial effect of inducing oxidative stress by increasing the generation of reactive oxygen species during oxidative phosphorylation[38,39]. The increased ciprofloxacin sensitivity observed in arginine-rich conditions may be attributed to the induction of biofilm formation during treatment. Arginine-induced biofilm formation imposes a high metabolic burden on the cells[40], aligning with the effective anti-biofilm activity of ciprofloxacin[41]. The difference in ciprofloxacin susceptibility among nutrient conditions might be due to a pH-dependent effect, although our medium was phosphate buffered to a pH of 7.4. Our observations in ciprofloxacin susceptibility correspond to previous findings of ciprofloxacin being more effective in alkaline conditions, e.g. arginine, compared to less sensitivity in acidic conditions, e.g. glutamate and aspartate[42]. However, this pH-mediated effect is not present in the observed reduced tobramycin susceptibility in arginine-rich conditions. Unbuffered arginine increases media alkalinity, resulting in increased tobramycin cellular uptake by increasing the transmembrane potential[43].

In our study, for tobramycin, we observed enhanced sensitivity for proline and glucose, whereas for lactate and alanine, reduced sensitivity was found. So far previous studies have only investigated the effect of glucose-enriched media on *P. aeruginosa* tobramycin sensitivity, finding a similar potentiation effect[44,45]. Cellular respiration is key for aminoglycoside uptake, thereby directly relating tobramycin susceptibility to energy metabolism[44]. The nutrients alternated in our media compositions are all closely linked to the TCA cycle, and intermediate products have been consistently correlated with tobramycin potentiation[18,44-46]. Interestingly, the sensitivity enhancement associated with TCA cycle activity can be suppressed by reducing the production of electron carriers through the activation of pleiotropic metabolic pathways. The redox imbalance induced by these alternative pathways and anaerobic energy production can be mitigated through the utilization of lactate[47]. This observation may provide an explanation for the reduced susceptibility in lactate-rich media. Although proline and alanine demonstrated a profound effect on tobramycin treatment in our study, and previous research highlighted their role in alternative energy-producing pathways such as denitrification[48,49], their exact role in *P. aeruginosa* metabolism during tobramycin treatment remains to be investigated.

Our PK-PD simulation illustrates how differences in PD response under nutrient-enriched conditions may lead to clinically relevant changes in antibiotic treatment response. This is demonstrated using a clinical tobramycin PK profile and the PD parameters from glucose and lactate-enriched conditions. While these in vitro conditions do not fully replicate *in vivo* growth environments, which may also involve phenotypical adaptations such as biofilm formation or interspecies interactions, they underscore the relevance of considering nutrient conditions in the infectious microenvironment. This is especially relevant when nutrient availability could be altered under specific disease conditions. For instance, elevated lactate levels have been found in CF patients with declining lung function[50], which could thus potentially contribute to the reduced tobramycin efficacy in adult CF patients[51]. Diabetes is a common disease in CF patients and for which increased glucose levels can be expected, which could potentially affect TOB treatment response[52].

The nutrient conditions employed in this study do not capture the full complexity of potential CF lung environments but provide isolated insights into the effect of specific nutrient conditions. Nutrients showed modest differential impact on bacterial fitness (μ_{max}) and profound changes in growth yield (N_{max}). The minimal impact on μ_{max} from substituting a single nutrient is consistent with prior studies on glucose and lactate addition to minimal media[53], and can be explained by a compressed nutrient utilization hierarchy under nutrient-poor conditions [54,55], facilitating the simultaneous utilization of the basal medium nutrients and the added nutrients. This efficient metabolic regulation of *P. aeruginosa* suggests that our findings may not directly extrapolate to other conditions or nutrient combinations. Future research, focusing specifically on nutrient utilization during antibiotic exposure, will be crucial to deepen our understanding of specific nutrients' roles in more complex environments.

In conclusion, our study demonstrates a profound impact of specific nutrient conditions on antibiotic sensitivity, with only modest effects on fitness. While broader clinical applicability of our results remains to be further elucidated, our work underscores the relevance of nutrients in the infectious microenvironment. Ultimately, it could be envisioned that specific nutrient levels in either plasma or sputum may be considered a clinically relevant predictor of antibiotic treatment response. Similarly, the effect of nutrient conditions may be important for consideration in antibiotic susceptibility testing.

3.5. References

1. M. Shteinberg, I.J. Haq, ... J.C. Davies (2021). Cystic fibrosis. *The Lancet* 397:2195–2211.

2. J.J. LiPuma (2022). The Sense and Nonsense of Antimicrobial Susceptibility Testing in Cystic Fibrosis. *Journal of the Pediatric Infectious Diseases Society* 11:S46–S52.

3. R. Somayaji, M.D. Parkins, ... D.R. VanDevanter (2019). Antimicrobial susceptibility testing (AST) and associated clinical outcomes in individuals with cystic fibrosis: A systematic review. *Journal of Cystic Fibrosis* 18:236–243.

4. C. Winstanley, S. O'Brien, M.A. Brockhurst (2016). Pseudomonas aeruginosa Evolutionary Adaptation and Diversification in Cystic Fibrosis Chronic Lung Infections. *Trends in Microbiology* 24:327–337.

5. J.D. Chandler, C.R. Esther (2022). Metabolomics of airways disease in cystic fibrosis. *Current Opinion in Pharmacology* 65:102238.

6. F. Rojo (2010). Carbon catabolite repression in *Pseudomonas* : optimizing metabolic versatility and interactions with the environment. *FEMS Microbiol Rev* 34:658–684.

7. K.L. Palmer, L.M. Aye, M. Whiteley (2007). Nutritional Cues Control Pseudomonas aeruginosa Multicellular Behavior in Cystic Fibrosis Sputum. *Journal of Bacteriology* 189:8079–8087.

8. A. Folkesson, L. Jelsbak, ... S. Molin (2012). Adaptation of Pseudomonas aeruginosa to the cystic fibrosis airway: an evolutionary perspective. *Nat Rev Microbiol* 10:841–851.

9. H. Lund-Palau, A.R. Turnbull, ... J.C. Davies (2016). *Pseudomonas aeruginosa* infection in cystic fibrosis: pathophysiological mechanisms and therapeutic approaches. *Expert Review of Respiratory Medicine* 10:685–697.

10. E. Rossi, R. La Rosa, ... H.K. Johansen (2021). Pseudomonas aeruginosa adaptation and evolution in patients with cystic fibrosis. *Nature Reviews Microbiology* 19:331–342.

11. S. Kirchner, J.L. Fothergill, ... C. Winstanley (2012). Use of Artificial Sputum Medium to Test Antibiotic Efficacy Against Pseudomonas aeruginosa in Conditions More Relevant to the Cystic Fibrosis Lung. *JoVE* 3857.

12. Y.D. Iglesias, F. Van Bambeke (2020). Activity of antibiotics against Pseudomonas aeruginosa in an in vitro model of biofilms in the context of cystic fibrosis: Influence of the culture medium. *Antimicrobial Agents and Chemotherapy* 64:1–14.

13. S.J. Mohammed, 1. Market Research and Consumer Protection Center, University of Baghdad, Baghdad, Iraq, ... 2. Central Public Health Laboratory, Ministry of Health, Baghdad, Iraq (2022). Comparison of three culture media in assessing the sensitivity of antibiotics to common foodborne microorganisms. *JMedLife* 15:645–649.

14. G. Manzo, F. Gianfanti, ... A.J. Mason (2021). Impacts of Metabolism and Organic Acids on Cell Wall Composition and *Pseudomonas aeruginosa* Susceptibility to Membrane Active Antimicrobials. *ACS Infect Dis* 7:2310–2323.

15. E. Deschamps, A. Schaumann, ... S. Alexandre (2021). Membrane

phospholipid composition of Pseudomonas aeruginosa grown in a cystic fibrosis mucus-mimicking medium. *Biochimica et Biophysica Acta (BBA) - Biomembranes* 1863:183482.

16. H. Liu, Y. Wang, ... X. Xie (2023). Nutrient condition modulates the antibiotic tolerance of Pseudomonas aeruginosa. *Science of The Total Environment* 904:166749.

17. S. Meylan, C.B.M. Porter, ... J.J. Collins (2017). Carbon Sources Tune Antibiotic Susceptibility in Pseudomonas aeruginosa via Tricarboxylic Acid Cycle Control. *Cell Chemical Biology* 24:195–206.

18. M. Koeva, A.D. Gutu, ... D. Joseph-McCarthy (2017). An Antipersister Strategy for Treatment of Chronic Pseudomonas aeruginosa Infections. *Antimicrob Agents Chemother* 61:e00987-17.

19. X. Bao, E. Goeteyn, ... T. Coenye (2023). Effect of malate on the activity of ciprofloxacin against *Pseudomonas aeruginosa* in different *in vivo* and *in vivo* -like infection models. *Antimicrob Agents Chemother* 67:e00682-23.

20. A. Brauner, O. Fridman, ... N.Q. Balaban (2016). Distinguishing between resistance, tolerance and persistence to antibiotic treatment. *Nat Rev Microbiol* 14:320–330.

21. B.A. Berryhill, T. Gil-Gil, ... B.R. Levin (2023). What's the Matter with MICs: Bacterial Nutrition, Limiting Resources, and Antibiotic Pharmacodynamics. *Microbiol Spectr* 11:e04091-22.

22. R.R. Regoes, C. Wiuff, ... B.R. Levin (2004). Pharmacodynamic Functions: a Multiparameter Approach to the Design of Antibiotic Treatment Regimens. *Antimicrob Agents Chemother* 48:3670–3676.

23. H.L. Rocchetta, C.J. Boylan, ... T.R. Parr (2001). Validation of a Noninvasive, Real-Time Imaging Technology Using Bioluminescent *Escherichia coli* in the Neutropenic Mouse Thigh Model of Infection. *Antimicrob Agents Chemother* 45:129–137.

24. G.R. Siragusa, K. Nawotka, ... C.H. Contag (1999). Real-Time Monitoring of *Escherichia coli* O157:H7 Adherence to Beef Carcass Surface Tissues with a Bioluminescent Reporter. *Appl Environ Microbiol* 65:1738–1745.

25. M. Kahm, G. Hasenbrink, ... M. Kschischo (2010). **grofit** : Fitting Biological Growth Curves with *R*. *J Stat Soft* 33.

26. C.W. Dunnett (1955). A Multiple Comparison Procedure for Comparing Several Treatments with a Control 50:1096–1121.

27. G. A. F. Seber, C. J. Wild Nonlinear Regression, p. 330. *In* .

28. A. Aminimanizani (2002). Distribution and elimination of tobramycin administered in single or multiple daily doses in adult patients with cystic fibrosis. *Journal of Antimicrobial Chemotherapy* 50:553–559.

29. Z.A. Noel, J. Wang, M.I. Chilvers (2018). Significant Influence of EC $_{50}$ Estimation by Model Choice and EC $_{50}$ Type. *Plant Disease* 102:708–714.

30. M.C. Walters, F. Roe, ... P.S. Stewart (2003). Contributions of Antibiotic Penetration, Oxygen Limitation, and Low Metabolic Activity to Tolerance of *Pseudomonas aeruginosa* Biofilms to Ciprofloxacin and Tobramycin. *Antimicrob Agents Chemother* 47:317–323.

31. S. Sauvage, C. Gaviard, ... J. Hardouin (2022). Impact of Carbon Source Supplementations on *Pseudomonas*

aeruginosa Physiology. *J Proteome Res* 21:1392–1407.

32. T. Fukuoka, N. Masuda, ... S. Ohya (1991). Increase in susceptibility of Pseudomonas aeruginosa to carbapenem antibiotics in low-amino-acid media. *Antimicrob Agents Chemother* 35:529–532.

33. H. Muramatsu, T. Horii, ... M. Maekawa (2003). Effect of basic amino acids on susceptibility to carbapenems in clinical Pseudomonas aeruginosa isolates. *International Journal of Medical Microbiology* 293:191–197.

34. J. Atrissi, A. Milan, ... C. Lagatolla (2021). Interplay of OpdP Porin and Chromosomal Carbapenemases in the Determination of Carbapenem Resistance/Susceptibility in Pseudomonas aeruginosa. *Microbiol Spectr* 9:e01186-21.

35. M.M. Ochs, C.-D. Lu, ... A.T. Abdelal (1999). Amino Acid-Mediated Induction of the Basic Amino Acid-Specific Outer Membrane Porin OprD from *Pseudomonas aeruginosa*. *J Bacteriol* 181:5426–5432.

36. C. Feehily, K.A.G. Karatzas (2013). Role of glutamate metabolism in bacterial responses towards acid and other stresses. *J Appl Microbiol* 114:11–24.

37. M.A. Alford, A. Baghela, ... R.E.W. Hancock (2020). NtrBC Regulates Invasiveness and Virulence of Pseudomonas aeruginosa During High-Density Infection. *Front Microbiol* 11:773.

38. M.A. Lobritz, P. Belenky, ... J.J. Collins (2015). Antibiotic efficacy is linked to bacterial cellular respiration. *Proc Natl Acad Sci USA* 112:8173–8180.

39. A. Gutierrez, S. Jain, ... J.J. Collins (2017). Understanding and Sensitizing Density-Dependent Persistence to Quinolone Antibiotics. *Molecular Cell* 68:1147-1154.e3.

40. T. Wassermann, K. Meinike Jørgensen, ... O. Ciofu (2016). The phenotypic evolution of Pseudomonas aeruginosa populations changes in the presence of subinhibitory concentrations of ciprofloxacin. *Microbiology* 162:865–875.

41. M. Žiemytė, M. Carda-Diéguez, ... M.D. Ferrer (2021). Real-time monitoring of *Pseudomonas aeruginosa* biofilm growth dynamics and persister cells' eradication. *Emerging Microbes & Infections* 10:2062–2075.

42. Z. Erdogan-Yildirim, A. Burian, ... M. Zeitlinger (2011). Impact of pH on bacterial growth and activity of recent fluoroquinolones in pooled urine. *Research in Microbiology* 162:249–252.

43. D. Lebeaux, A. Chauhan, ... J.-M. Ghigo (2014). pH-Mediated Potentiation of Aminoglycosides Kills Bacterial Persisters and Eradicates In Vivo Biofilms. *The Journal of Infectious Diseases* 210:1357–1366.

44. S. Meylan, C.B.M. Porter, ... J.J. Collins (2017). Carbon Sources Tune Antibiotic Susceptibility in Pseudomonas aeruginosa via Tricarboxylic Acid Cycle Control. *Cell Chemical Biology* 24:195–206.

45. C.W. Hall, E. Farkas, ... T.-F. Mah (2019). Potentiation of Aminoglycoside Lethality by C_4-Dicarboxylates Requires RpoN in Antibiotic-Tolerant Pseudomonas aeruginosa. *Antimicrob Agents Chemother* 63:e01313-19.

46. A. Crabbé, L. Ostyn, ... T. Coenye (2019). Host metabolites stimulate the bacterial proton motive force to enhance the activity of aminoglycoside antibiotics. *PLoS Pathog* 15:e1007697.

47. Y.-C. Lin, W.C. Cornell, ... L.E.P. Dietrich (2018). The Pseudomonas aeruginosa Complement of Lactate Dehydrogenases Enables Use of D - and L -Lactate and Metabolic Cross-Feeding. *mBio* 9:e00961-18.

48. S.L. Christgen, D.F. Becker (2019). Role of Proline in Pathogen and Host Interactions. *Antioxidants & Redox Signaling* 30:683–709.

49. S. Kuang, Y. Chen, ... H. Li (2021). Synergy of alanine and gentamicin to reduce nitric oxide for elevating killing efficacy to antibiotic-resistant *Vibrio alginolyticus*. *Virulence* 12:1737–1753.

50. J. Phan, T. Gallagher, ... K. Whiteson (2018). Fermentation products in the cystic fibrosis airways induce aggregation and dormancy-associated expression profiles in a CF clinical isolate of Pseudomonas aeruginosa. *FEMS Microbiology Letters* 365.

51. D.E. Geller, S.Z. Nasr, ... M. Higgins (2014). Tobramycin Inhalation Powder in Cystic Fibrosis Patients: Response by Age Group. *Respir Care* 59:388–398.

52. A.L. Brennan, K.M. Gyi, ... E.H. Baker (2007). Airway glucose concentrations and effect on growth of respiratory pathogens in cystic fibrosis. *Journal of Cystic Fibrosis* 6:101–109.

53. C. Pajon, M.C. Fortoul, ... R.P. Smith (2023). Interactions between metabolism and growth can determine the co-existence of Staphylococcus aureus and Pseudomonas aeruginosa. *eLife* 12:e83664.

54. V. Behrends, T.M.D. Ebbels, ... J.G. Bundy (2009). Time-Resolved Metabolic Footprinting for Nonlinear Modeling of Bacterial Substrate Utilization. *Appl Environ Microbiol* 75:2453–2463.

55. R. La Rosa, V. Behrends, ... F. Rojo (2016). Influence of the Crc regulator on the hierarchical use of carbon sources from a complete medium in *P seudomonas*: Crc and the hierarchy of substrate consumption. *Environ Microbiol* 18:807–818.

3.6. Supplementary figures and tables

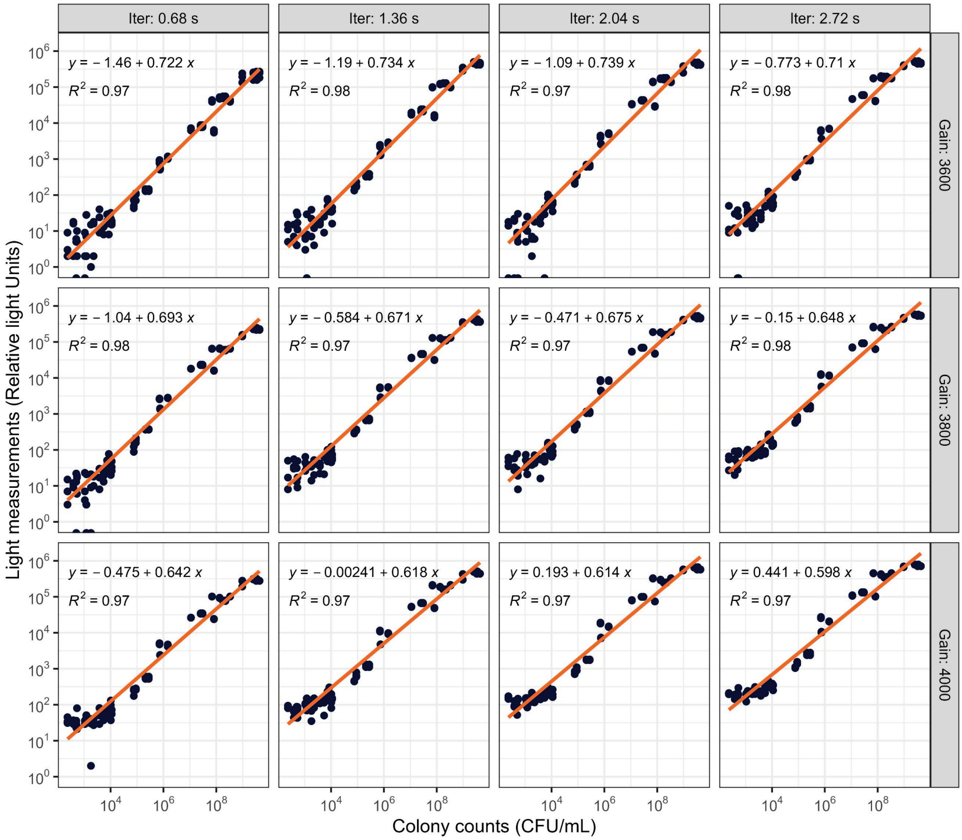

Supplemental Figure 1. Linear calibration between luminescence (relative light units, RLU) and cell counts (CFU/mL) for multiple combinations of detector settings, varying iteration time (iter, columns) and gain (rows). The iteration time stands for the total measurement time per well and the gain is amplification in the conversion from light into electric signal.

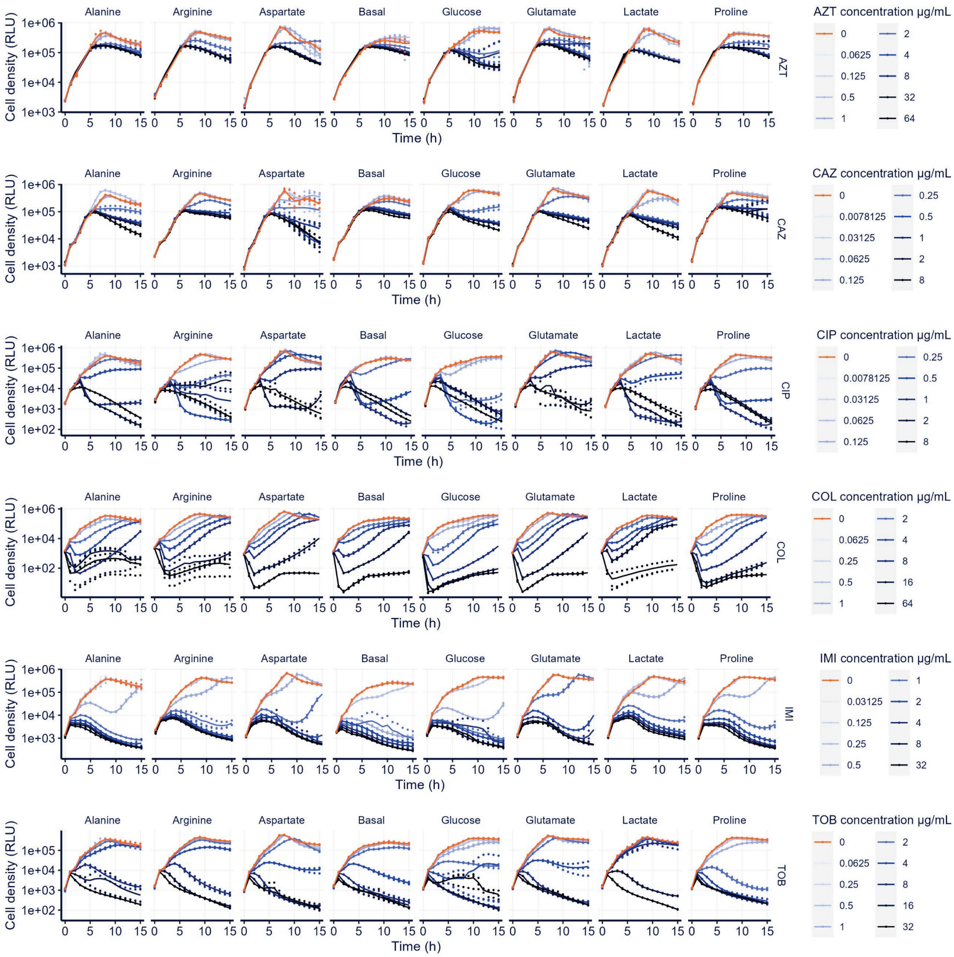

Supplemental figure 2. Dynamic analysis of the population size over time during the treatment of 6 antibiotics with 9 concentrations and a positive control in 8 media formulations. The y-axis is the cell density measured by relative light units (RLU). All conditions have 3 biological replicates. Abbreviations: aztreonam (AZT), ceftazidime (CAZ), ciprofloxacin (CIP), colistin (COL), imipenem (IMI), and tobramycin (TOB).

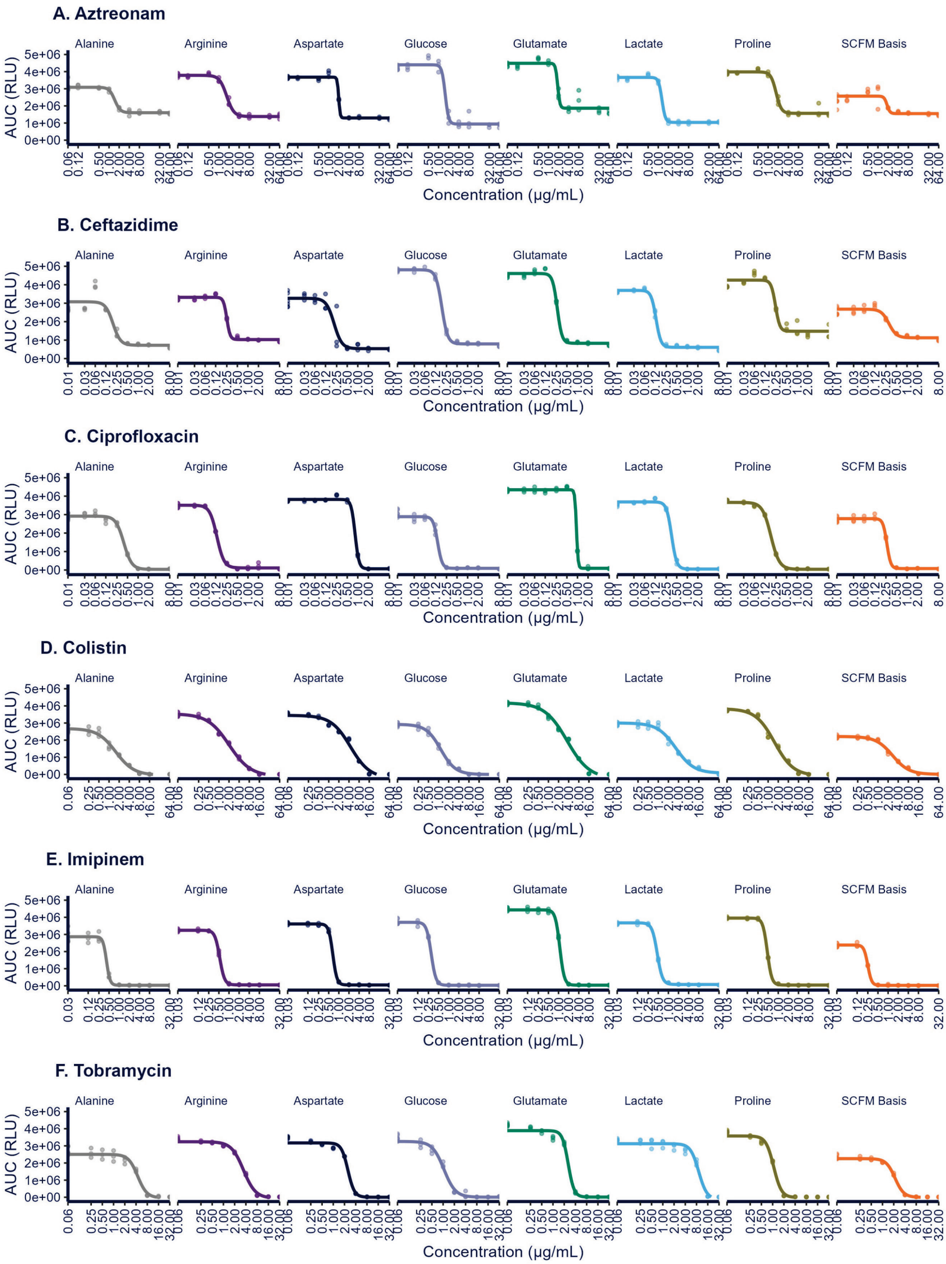

Supplemental Figure 3. Emax model fitting was performed on the area under the curve (AUC) of growth curves across varying antibiotic concentrations. The model was fitted using the average AUC values for each antibiotic concentration (n = 3). From this model, the upper limit (E0), the half-maximal effective concentration (EC50), and the lower limit (Emax) were determined.

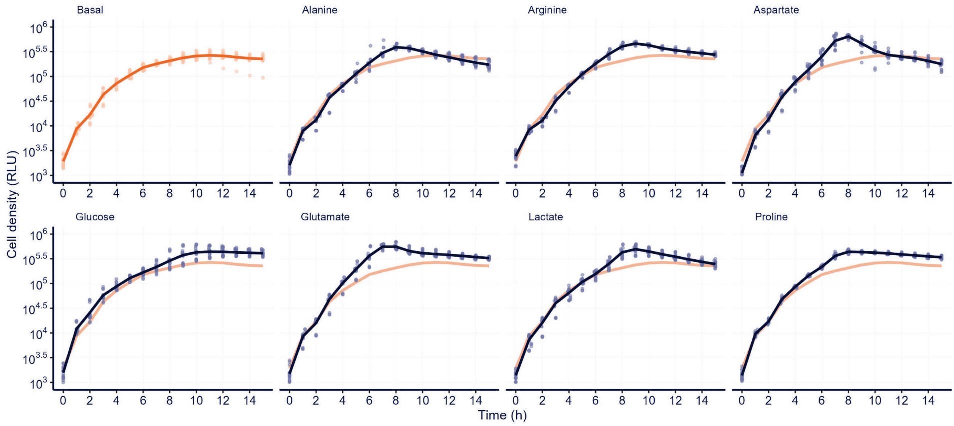

Supplemental figure 4. The dynamic effect of the addition of nutrients (navy blue lines) to the basal (orange) media composition on the population size over 15-hours of incubation in antibiotic free conditions.

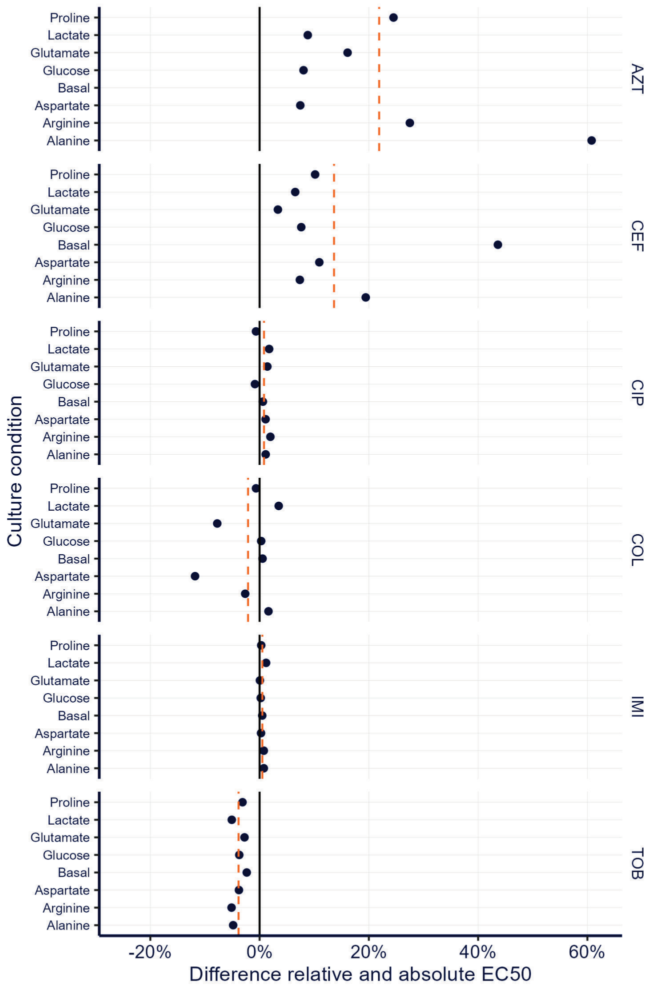

Supplemental figure 5. The difference between the relative half-maximal effective concentration (EC_{50}) and the absolute EC_{50}. The relative EC_{50} is extracted as the halve maximal response of the dose-response curve between the population fitness (E0) and the maximal drug effect (Emax). The absolute EC50 is extracted as the concentration at 50% reduction of E0. The difference between the two antibiotic sensitivity determinations is obtained by dividing the relative EC_{50} by the absolute EC_{50} concentrations per culture condition. Abbreviations: aztreonam (AZT), ceftazidime (CAZ), ciprofloxacin (CIP), colistin (COL), imipenem (IMI), and tobramycin (TOB).

A

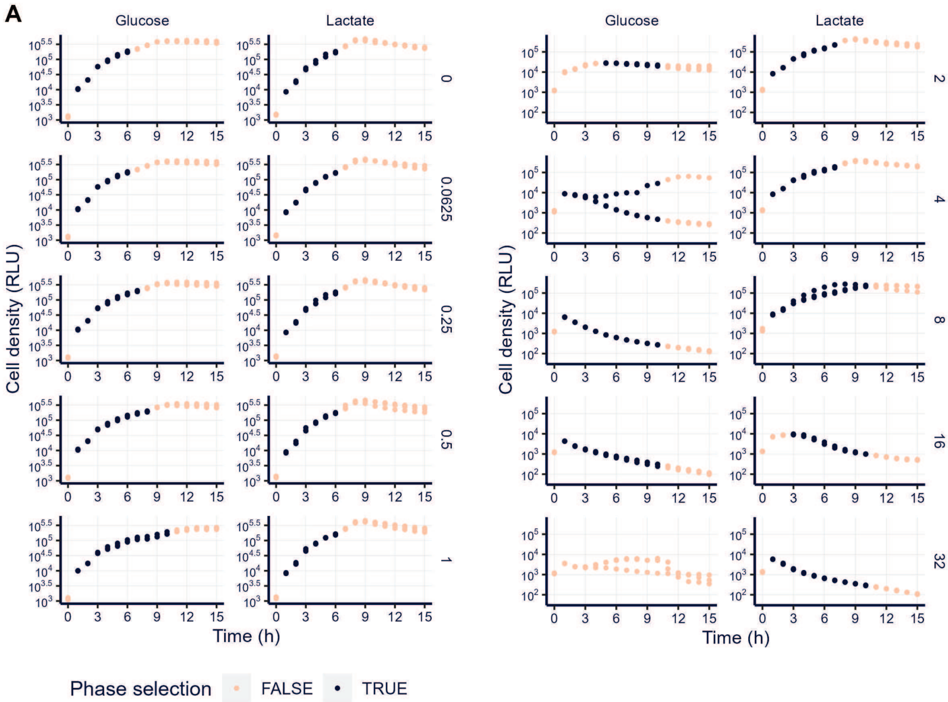

B

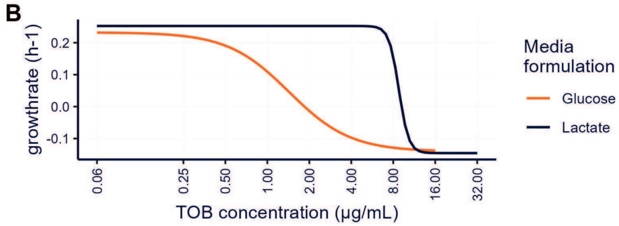

C

Parameter	Glucose	Lactate
EC50	1.41	8.58
µmax	0.24	0.25
Emax	-0.14	-0.15
Hill	1.85	16.06

Supplemental figure 6. Phase selection for growth rate determination for growth rate based dose-response modeling of tobramycin (TOB). (**A**) The time-points included (blue dots) for the determination of the growth or kill rate of the tobramycin concentration using a linear regression. (**B**) The sigmoid E_{max} dose-response curve for glucose and lactate using the growth rate as response. (**C**) The pharmacodynamic parameters extracted from the dose-response model.

Supplemental table 1. Detailed content list of synthetic media

	Name	Concentration (mM)	Company information
M9 buffer	di-sodium hydrogen phosphate (Na_2HPO_4)	90.2	Thermo Fisher Scientific
	Potassium di-hydrogen phosphate (KH_2PO_4)	22.0	VWR International
	Sodium chloride (NaCl)	8.5	Merck KGaA (Avantor™)
	Ammonium chloride (NH_4Cl)	18.6	Alfa Aesar
	Magnesium sulphate hepta-hydrate ($MgSO_4$)	1.0	VWR International
	Calcium chloride ($CaCl_2$)	0.1	Acros Organics
Salts	Potassium nitrate (KNO_3)	0.35	Acros Organics
	Iron sulphate ($FeSO_4$)	0.0036	Alfa Aesar
Suppl.	BME Vitamin solution	*1x*	Thermo Fisher Scientific
Trace metals	Di-sodium Ethylene di-amine tetra-acetic acid (EDTA)	0.002 (mg/mL)	J.T. Baker (Avantor™)
	Zinc Sulphate hepta-hydrate ($ZnSO_4$)	0.23 (mg/mL)	Alfa Aesar
	Boric acid (H_3BO_3)	0.111 (mg/mL)	Acros Organics
	Manganese chloride tetra-hydrate ($MnCl_2$)	0.051 (mg/mL)	Sigma Aldrich (Avantor™)
	Cobalt chloride ($CoCl_2$)	0.017 (mg/mL)	Alfa Aesar
	Copper Sulphate penta-hydrate ($CuSO_4$)	0.015 (mg/mL)	Sigma Aldrich (Avantor™)
	Ammonium hepta-molybdate tetra hydrate ($(NH_4)_6\ Mo_7O_2$)	0.01 (mg/mL)	Alfa Aesar
Basis nutrients	Cysteine (Cys)	0.2	Chem-Impex International
	Glycine (Gly)	1.2	Acros Organics
	Histidine hydrochloride (His)	0.5	Chem-Impex International
	Isoleucine (Ile)	1.1	Chem-Impex International
	Leucine (Leu)	1.6	Chem-Impex International
	Lysine hydrochloride (Lys)	2.1	Thermo Fisher Scientific
	Methionine (Met)	0.6	Chem-Impex International
	Phenylalanine (Phe)	0.5	Chem-Impex International
	Serine (Ser)	1.4	Chem-Impex International
	Threonine (Thr)	1.0	Chem-Impex International
	Tryptophan (Trp)	0.01	Chem-Impex International
	Tyrosine (Tyr)	0.8	Chem-Impex International
	Valine (Val)	1.1	Chem-Impex International
Nutrient alterations	Alanine (Ala)	15	Chem-Impex International
	Arginine (Arg)	15	Chem-Impex International
	Aspartate (Asp)	15	Chem-Impex International
	Glutamate (Glu)	15	Chem-Impex International
	Sodium lactate (LAC)	15	Biosynth International
	Proline (Pro)	15	Thermo Fisher Scientific
	Glucose (GLC)	15	Alfa Aesar

Supplemental table 2. Pharmacokinetic parameters

Explanation	Name	Value / Formula	Unit
Patient bodyweight	BW	55.3	kg
Patient age		29.0	years
Clearance rate per BW	CL_t	0.1212	L/h/kg
Volume comp. 1 per BW	V_C	0.20	L/kg
Distribution rate per BW	CL_d	0.0702	L/h/kg
Volume comp. 2 per BW	V_{ss}	0.38	L/kg
Individual Variability (η)	η_{CL_t} η_{V_C} η_{CL_d} $\eta_{V_{ss}}$	28.5 28.2 66.6 27.8	% % % %
Population size		1000	
Dosing interval		8	h
Dosing amount		$3.3 * BW$	mg
Dosing duration		0.30	h
Volume compartment 1	$V_{central}$	$V_C * e^{\{iv\}} * BW$	L
Elimination rate from $V_{central}$	$k_{elimination}$	$(CL_t * e^{\{iv\}} * BW) / V_{central}$	
Volume compartment 2	V_2	$V_{ss} * e^{\{iv\}} * BW$	L
Rate constant 1-->2	K_{12}	$(CL_d * e^{\{iv\}} * BW) / V_{central}$	
Rate constant 2-->1	K_{21}	$(CL_d * e^{\{iv\}} * BW) / V_2$	
Amount in compartment 1	$m_{central}$	$\frac{m_{central}(t)}{dt} = k_{21} * m_2 - (k_{elimination} + k_{12}) * m_{central}$	mg
Amount in compartment 2	m_2	$\frac{m_2(t)}{dt} = K_{12} * m_{central}(t) - k_{21} * m_2(t)$	mg
Concentration compartment 1	$C_{central}$	$m_{central} / V_{central}$	mg/L

Explanations	Name	Value / Formula		Unit
		Glucose	Lactate	
Max. drug effect	E_{max}	-0.144	-0.146	h^{-1}
Max. growth rate	K_{growth} (E_0)	0.240	0.254	h^{-1}
Half effective concentration	EC_{50}	1.406	8.582	mg/L
Hill coefficicent	n_H	1.850	16.057	
Starting population	N_0	$1 * 10^6$		CFU/mL
Max. population	N_{max}	$9 * 10^9$		CFU/mL
Effective growth rate	k_{effect}	$K_{growth} - (E_{max} + \frac{K_{growth} - E_{max}}{1 + e^{n_H(\log(C_{central}) - \log(EC_{50}))}})$		h^{-1}
Infection population	N(t)	$\frac{dN(t)}{dt} = (k_{growth} * (1 - N(t)/N_{max}) - k_{effect}) * N(t)$		CFU/mL

Supplemental table 3. Pharmacodynamic parameters